Mean lifetime measurements and calculations of long-lived $HeNe^{2+}$ isotopes

I. Ben-Itzhak,[1] J. P. Bouhnik,[2] Z. Chen,[1,*] B. D. Esry,[3] I. Gertner,[2] C. Heinemann,[4,†] W. Koch,[4] C. D. Lin,[1] and B. Rosner[2]

[1]*J.R. Macdonald Laboratory, Department of Physics, Kansas State University, Manhattan, Kansas 66506*

[2]*Department of Physics, Technion, Haifa 32000, Israel*

[3]*Department of Physics, JILA, University of Colorado, Boulder, Colorado 80309*

[4]*Institut für Organische Chemie, Technische Universität Berlin, Strasse des 17. Juni 135, D-10623 Berlin, Germany*

(Received 18 December 1996)

The mean lifetimes of the $^3He\,^{20}Ne^{2+}$ and $^3He\,^{22}Ne^{2+}$ isotopes of the $HeNe^{2+}$ molecular ion have been measured to be 55 ± 10 ns and 72 ± 14 ns, respectively. These mean lifetimes are similar to each other and about a factor of 3 smaller than the previously reported mean lifetime of the most abundant $^4He\,^{20}Ne^{2+}$ isotope. The small differences between the mean lifetimes of the different isotopes suggest that the long-lived $HeNe^{2+}$ decays mainly by dipole electronic transitions to lower dissociating states. We have performed multireference configuration interaction (MRCI) calculations of the $HeNe^{2+}$ ground state and many excited electronic states. The electronic ground state is found to be metastable and deep enough to sustain a single vibrational state in contrast to previous calculations. However, its calculated mean lifetime is $\sim$11 ps which is too short to be detected in our experiments. Excited states associated with the $He + Ne^{2+}$ dissociation limits are bound by the long-range interaction between Ne^{2+} and polarized He. Similarly, the lowest state associated with a $He^{2+} + Ne$ dissociation limit is also bound by long-range interaction. Due to an avoided crossing, the singlet state correlating with the first excited $He^{+} + Ne^{+}$ limit is metastable. These states decay mainly by dipole electronic transitions to lower dissociating states. Decay rate calculations suggest five possible electronic states which are in agreement with the measured values. [S1050-2947(97)05608-4]

PACS number(s): 31.50.+w, 34.50.Gb

I. INTRODUCTION

A couple of years ago, we reported that long-lived states of $^4He\,^{20}Ne^{2+}$ are formed in charge-stripping collisions between 900 keV $^4He\,^{20}Ne^{+}$ and Ar atoms, and that the mean lifetime of the most abundant isotope is 184 ± 32 ns [1]. At that time the low-lying $^1\Sigma^+$ electronic states of this molecular ion had been investigated using configuration interaction [2] and many-body perturbation [3] theories. Only the lowest of these states has a local minimum, but the calculated potential-energy curves are too shallow to support any vibrational levels. Thus, it was suggested that the observed long-lived $HeNe^{2+}$ was formed in bound or metastable highly excited electronic states [1]. In particular, states of different symmetry than the $^1\Sigma^+$ symmetry of the electronic ground state were considered to be likely candidates. This was based on the assumption that states of the same symmetry will decay to the ground state and dissociate much faster than the measured mean lifetime.

Not only was the long-lived electronic state not identified, but also the decay mechanism of the $HeNe^{2+}$ was then unknown. It is possible that these molecular ions are formed in a bound excited state and then decay by dipole transitions to a lower unbound state which then rapidly dissociates. Given the long mean lifetimes, i.e., the small transition rates, this implies that the initial and final states are only weakly coupled. Another possibility is that a metastable state is populated for which dipole transitions are either forbidden or very slow. This metastable state then decays by tunneling through the potential-energy barrier. For the latter decay mechanism, large isotopic effects are expected as a result of the shift of the vibrational energy levels caused by the change of the reduced mass. Thus, mean lifetime measurements of different isotopes can indicate which decay mechanism is more likely. Such measurements have been used recently to determine the decay mechanism of $NeAr^{2+}$ [4]. In Sec. II measurements of the mean lifetimes of two other $HeNe^{2+}$ isotopes, namely, $^3He\,^{20}Ne^{2+}$ and $^3He\,^{22}Ne^{2+}$, are presented. These measurements were done using the same method we used previously [1], and the results discussed in Sec. IV suggest that the long-lived $HeNe^{2+}$ decays by dipole transitions to lower dissociating states.

In order to determine which state of the $HeNe^{2+}$ molecular ion was the measured long-lived one, we have performed extensive *ab initio* multireference configuration interaction calculations which are described in Sec. III A. The local minimum of the newly calculated ground electronic state is much deeper than suggested by previous calculations [2,3]. This local minimum can sustain a single vibrational state. Its mean lifetime, however, is too short to be detected in our measurements. Among the calculated potential-energy curves there are a few possible long-lived states. We have calculated the decay rates by tunneling and by dipole transitions of all those bound and metastable states (see Sec. III B). The calculated mean lifetimes are compared to the measured ones in Sec. IV.

*Present address: Siemens Medical Systems, 4040 Nelson Avenue, Concord, CA 94520.

†Present address: Hoechst AG, D-65926 Frankfurt am Main, Germany.

II. EXPERIMENT

The mean lifetimes of the $^3He\,^{20}Ne^{2+}$ and $^3He\,^{22}Ne^{2+}$ isotopes have been determined using the same experimental method that was used by us previously to measure the most abundant $^4He\,^{20}Ne^{2+}$ isotope [1], thus it will be described only briefly. The $HeNe^{2+}$ molecular ions were formed by charged-stripping collisions of 900 keV $HeNe^+$ with Ar. The different isotopes of the $HeNe^+$ parent molecular ions were formed in the accelerator rf ion source which contained a mixture of He and Ne isotopes. The isotope of interest in each measurement was then selected by an analyzing magnet and directed through the differentially pumped target cell. The doubly charged molecular ions thus formed were then deflected toward a surface barrier detector by a parallel plate electrostatic analyzer. The number of $HeNe^{2+}$ which dissociated in flight after the analyzer was determined from the number of He fragments detected. These fragments have only a small fraction of the beam energy ($\frac{3}{23}E_{\mathrm{Beam}}$ for the $^3He\,^{20}Ne^{2+}$, for example) and can be distinguished from the other fragments, molecules, and atoms taking advantage of the fact that the detector produces a signal proportional to the particle energy. To assure that the He fragments will not coincide with the Ne fragment from the dissociation of the same molecule a mask covering half the detector was used. (Note that the fragments of a diatomic molecule move in opposite directions in the center-of-mass frame, and thus, if half the detector is covered only one of them can be detected). For details see [1,5].

The number of detected He fragments from the dissociation in flight after the analyzer of the $HeNe^{2+}$ molecular ions is given in Fig. 1 for the different isotopes. (The $^4He\,^{20}Ne^{2+}$ data are taken from Ref. [1]). The data were fitted assuming a single exponential decay which yields the following expression:

$$N(\mathrm{He}) = \tfrac{1}{2}N_0[e^{-x/v\tau} - e^{-l_d/v\tau}], \tag{1}$$

where N_0 is the number of $HeNe^{2+}$ formed in the target cell, x and l_d are the distances from the target cell to the analyzer exit and the detector, respectively, v is the beam velocity, and τ is the effective mean lifetime [1,5].

III. THEORETICAL METHODS

A. Potential-energy curves

The low-lying molecular states of the $HeNe^{2+}$ system which we investigated by *ab initio* quantum chemical molecular orbital calculations and the associated dissociation channels [6] are given in Table I. It should be noted that a series of atomic asymptotes is located between the asymptotes V and VI from Table I corresponding to $He^+ + Ne^{+}*$, where a nonvalence excited state of the neon atom is involved, such as $2s^2\,2p^4\,x^1$ with $x = 3s, 3p$, etc. These states were not included in our investigation, since (i) they are expected to be completely repulsive (due to the large size of $Ne^{+}*$) and (ii) the one-particle description employed, although quite extensive (see below), is not optimized with respect to an adequate description of such nonvalence excited states of the atom and the corresponding molecular Rydberg states. Adiabatic potential-energy curves for all states included in Table I were calculated using the complete-active space self-consistent field (CAS-SCF) [7] and multireference configuration interaction method (MRCI) [8]. In this approach, the zeroth-order wave function is generated by including all symmetry-adapted configuration state functions obtained by distributing the eight valence electrons in 2–4σ and 1π molecular orbitals built from the $2s,2p$(Ne) and $1s$(He) atomic orbitals [the $1s$ (Ne) orbital was kept doubly occupied]. Natural CAS-SCF orbitals were individually optimized for each electronic state and subsequently employed in the MRCI treatment, which covered all single and double excitations from the reference space described above (the $1s$ electrons of Ne were not correlated). The MRCI total energies E_{MRCI} were corrected by the renormalized multireference Davidson correction [9] to obtain final energies $E_{\mathrm{MRCI}+Q}$, which are approximately size extensive

$$E_{\mathrm{MRCI}+Q} = E_{\mathrm{MRCI}} + \Delta E_c \frac{1 - c_0^2}{c_0^2}. \tag{2}$$

Here, ΔE_c denotes the energy difference between the MRCI energy and the energy of the CAS-SCF reference wave function, and c_0 is the weight of the reference space in the total MRCI expansion.

For the expansion of the molecular orbitals, a Gaussian basis set of the atomic natural orbital (ANO) [10] type was used. Following Widmark, Persson, and Roos [[10](b)], a $[7s7p4d3f]$ contraction of a $(14s9p4d3f)$ primitive set was employed for neon and supplemented by two g-type functions with exponents of 3.18 and 1.272 (generated by an even-scaling procedure from one g exponent, energy optimized for the neon atom in a configuration interaction calculation with all single and double excitations). The corresponding helium basis has $[7s4p3d2f]$ contracted functions from a $(9s4p3d2f)$ primitive set. Only the pure spherical harmonic components of the basis functions were used, thus the one-particle set includes a total of 135 contracted Gaussian functions. Transition dipole moments between the different electronic states of $HeNe^{2+}$ were calculated from the CAS-SCF wave functions employing the CAS state interaction method [11] to avoid errors due to the nonorthogonality of the CAS-SCF wave functions of the same symmetry. All calculation were performed with the MOLCAS-2 and -3 suites of quantum chemistry programs [12] on IBM RS/6000 workstations.

Atomic test calculations (see Table II) demonstrate the performance of the MRCI method and the employed one-particle basis for properties of interest for the present context. For the prediction of atomic energy levels [13], the largest error occurs in the second ionization energy of the neon atom, which is underestimated by 0.22 eV due to the incomplete treatment of the correlation energy. However, for the present purpose this accuracy in the ionization energies is acceptable on the background of the additional computational efforts associated with a further extension of the already fairly large basis sets to higher l-quantum numbers and of the n-particle space treatment, which would be required to bring the calculated ionization energies in better agreement with experiment. Considerably lower errors (max. 0.05 eV) occur for the electronic excitation energies of the neon ions, which provides confidence in the performance of the MRCI method for the treatment of the electronically excited states

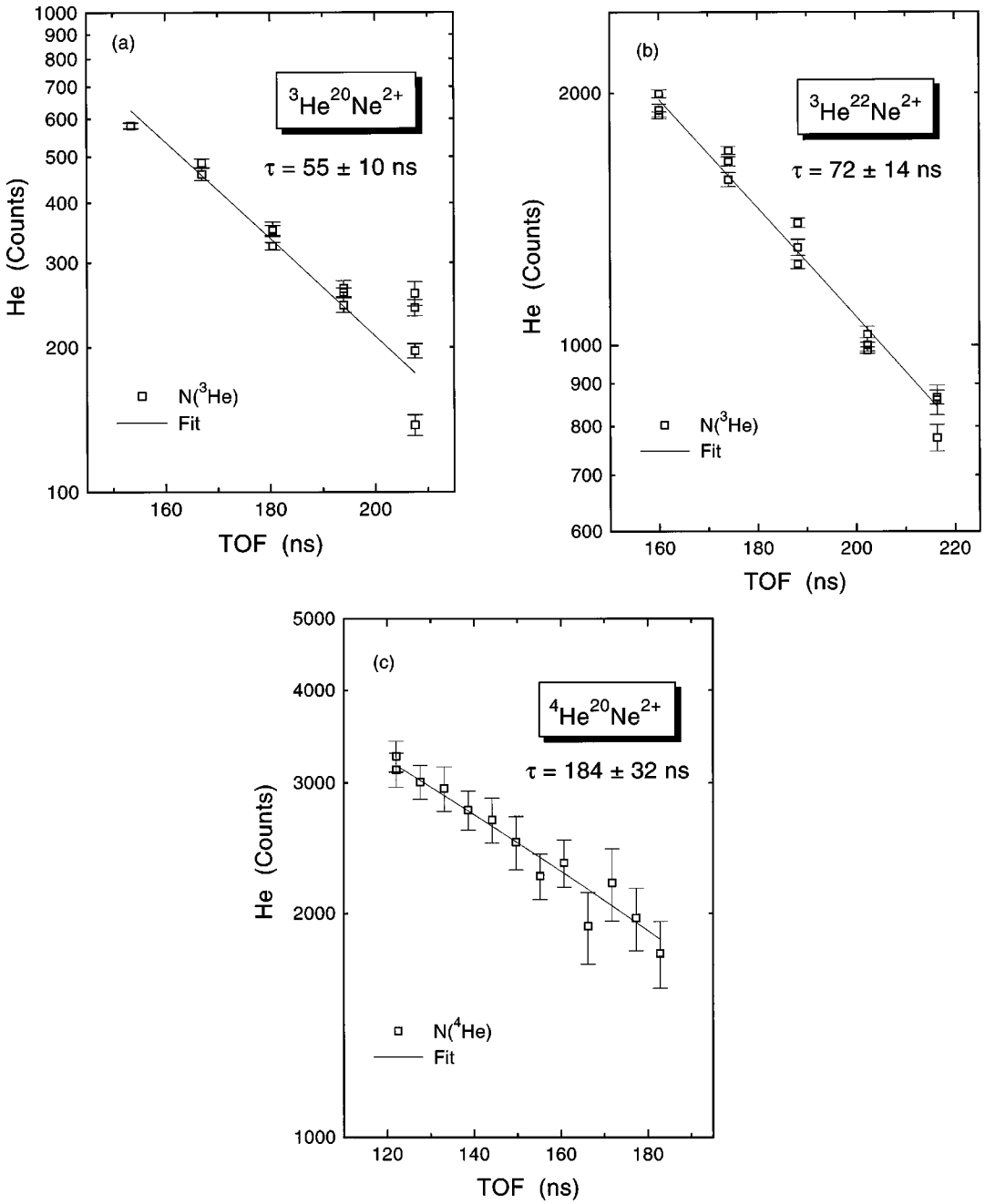

FIG. 1. The number of (a) ^{3}He ^{20}Ne^{2+}, (b) ^{3}He ^{22}Ne^{2+}, and (c) ^{4}He ^{20}Ne^{2+} (the data were taken from Ref. [1]) molecular ions, which passed the electrostatic analyzer, as a function of their flight time from the target cell. [The error bars on (a) and (b) represent statistical errors only.]

of HeNe^{2+}. Finally, the calculated dipole polarizability of the helium atom almost matches the experimental value while the respective MRCI+Q result for neon underestimates the experimental result by 4%, which is satisfactory for our purpose. Note that the SCF dipole polarizability in the employed basis amounts to 2.30 a.u., 0.07 a.u. lower than the SCF limit [14]. Based on earlier studies [14], most of the discrepancy between our MRCI+Q value of the dipole polarizability and the experimental number must be attributed to basis set incompleteness, in particular the lack of additional diffuse s and p functions.

Further information on the performance of the employed methods comes from a calculation on the $X\,^2\Sigma^+$ ground state of the singly charged HeNe$^+$ ion (Table III, see below). Solving the nuclear Schrödinger equation in the respective MRCI+Q potential, we obtain the following spectroscopic constants: R_e=2.702 a.u.; D_e=0.707 eV; and ω_e=956 cm^{-1}. Unfortunately, the HeNe$^+$ ground-state's experimental data seem not to be completely settled [15], but our theoretical results compare well to earlier MRD-CI calculations in the slightly smaller basis sets of Gemein, deVivie, and Peyerimhoff [[15](b)] who obtained R_e=2.67 a.u., D_e=0.70 eV, and ω_e=857 cm^{-1}. A final test on the accuracy of the MRCI method for the treatment of electron correlation was performed for part of the $X\,^1\Sigma^+$ ground-state potential-energy curve of HeNe^{2+}. In contrast to earlier the-

TABLE I. Theoretically investigated electronic states of $HeNe^{2+}$.

Dissociation limit	Label	Relative energy (eV)[a]	Associated molecular states
$He^+(^2S)+Ne^+(^2P)$	I	0.00	$X\,^1\Sigma^+$, $A\,^1\Pi$, $a\,^3\Pi$, $b\,^3\Sigma^+$
$He(^1S)+Ne^{2+}(^3P)$	II	16.50	$c\,^3\Sigma^-$, $d\,^3\Pi$
$He(^1S)+Ne^{2+}(^1D)$	III	19.66	$B\,^1\Delta$, $C\,^1\Pi$, $D\,^1\Sigma^+$
$He(^1S)+Ne^{2+}(^1S)$	IV	23.37	$E\,^1\Sigma^+$
$He^+(^2S)+Ne^+(^2S)$	V	26.88	$F\,^1\Sigma^+$, $e\,^3\Sigma^+$
$He^{2+}+Ne(^1S)$	VI	32.81	$G\,^1\Sigma^+$

[a]Atomic term energies are weighted averages over the individual J levels from Ref. [13].

oretical work using the configuration interaction method with significantly smaller basis sets [2], we find that both a distinct local minimum and local maximum, instead of only a broad shoulder, occur at around 2.0 and 2.5 a.u., respectively. The resulting metastable region of the potential-energy curve supports a single vibrational level which was localized using the Numerov method. The MRCI+Q potential-energy curve for this region is plotted in Fig. 2 together with the corresponding curves calculated from two single-reference Hartree-Fock (HF) based methods: (i) the coupled cluster approximation including all single and double excitations and a perturbative estimate of the triple excitations [16] [CCSD(T)], and (ii) the modified coupled-pair functional (MCPF) approach [17]. For cases in which the Hartree-Fock determinant represents already a good zeroth-order wave function of the system, the former approach usually picks up at least as much of the correlation energy as the MRCI scheme, while the latter is somewhat less rigorous but has been included since MCPF has frequently been used in similar calculations. If there were large differences between the potential-energy curves resulting from the three computational schemes, this would point to degeneracy problems in the wave function or to deficiencies in the treatment of the dynamical electron correlation. The corresponding total energies are given in Table IV. First note that in terms of total energies in the metastable region, the MRCI+Q and CCSD(T) approaches deviate by *at most 1* mH, and thus the corresponding parts of the potential energy are quite similar. The total well depth is 182 meV in the MRCI+Q potential-energy curve and 142 meV in the CCSD(T) potential-energy curve. The location of the minimum is quite similar with both methods [2.000 a.u. MRCI+Q and 1.998 a.u. CCSD(T)], while the CCSD(T) maximum is at a slightly shorter He-Ne internuclear distance, consistent with the lower barrier height. The good qualitative and quantitative agreement with the CCSD(T) calculation suggests that the chosen MRCI+Q method for the calculation of the potential-energy curves should be reliable in terms of the treatment of dynamical electron correlation. On the other hand, the MCPF calculation recovers a significantly smaller fraction of the correlation energy (5–9 mH in the metastable region) albeit the qualitative shape of the metastable potential-energy curve is very similar to the other two methods (barrier height of 226 meV, minimum at 1.987 a.u., and maximum at 2.508 a.u.).

The MRCI expansions for all calculated electronic states

TABLE II. Results from atomic calibration calculations.

Ionization energies	Calc. MRCI+Q method	Expt. [a]
$Ne(^1S)\rightarrow Ne^+(^2P)+e^-$	21.47 eV	21.59 eV
$Ne^+(^2P)\rightarrow Ne^{2+}(^3P)+e^-$	40.86 eV	41.08 eV
$He(^1S)\rightarrow He^+(^2S)+e^-$ [b]	24.57 eV	24.59 eV
Atomic excitation energies		
$Ne^+(^2P)\rightarrow Ne^+(^2S)$	26.81 eV	26.86 eV
$Ne^{2+}(^3P)\rightarrow Ne^{2+}(^1D)$	3.19 eV	3.16 eV
$Ne^{2+}(^3P)\rightarrow Ne^{2+}(^1S)$	6.88 eV	6.87 eV
Atomic dipole polarizabilities		
Ne	2.56 a.u.	2.67 a.u. [c]
He [b]	1.37 a.u.	1.38 a.u. [c]

[a]Atomic term energies are weighted averages over the individual J levels from Ref. [13] since spin-orbit coupling was not included in the calculations.
[b]Since the helium atom is a two-electron system, the $+Q$ correction was not used.
[c]Reference [23].

TABLE III. The $X\,^2\Sigma^+$ electronic ground-state potential-energy curve of $HeNe^+$.

R(a.u.)	E(a.u.)
2.00	−130.920 022
2.30	−130.973 923
2.50	−130.985 886
2.60	−130.988 269
2.70	−130.988 996
2.80	−130.988 504
2.90	−130.987 272
3.00	−130.985 621
3.20	−130.981 769
3.50	−130.976 473
3.70	−130.973 558
4.00	−130.970 468
5.00	−130.966 321
6.00	−130.965 381
9.00	−130.964 774
50.00	−130.963 023

are listed in Table V at $R=3.0$ a.u. The calculated potential-energy curves of the ground and excited electronic states of $HeNe^{2+}$ are presented in Fig. 3. The incomplete set of MRCI+Q numbers for the G state shown in Fig. 4 is due to severe root flipping problems in the CAS-SCF orbital optimization. The G and F states have been also calculated using the ground state CAS-SCF orbitals with no optimization (labeled MRCI in Fig. 4) as explained in further detail below. The numerical potential-energy values are tabulated on the e-PAPS system [18]. Finally, the transition dipole moments between the different electronic states of $HeNe^{2+}$ are given in Table VI.

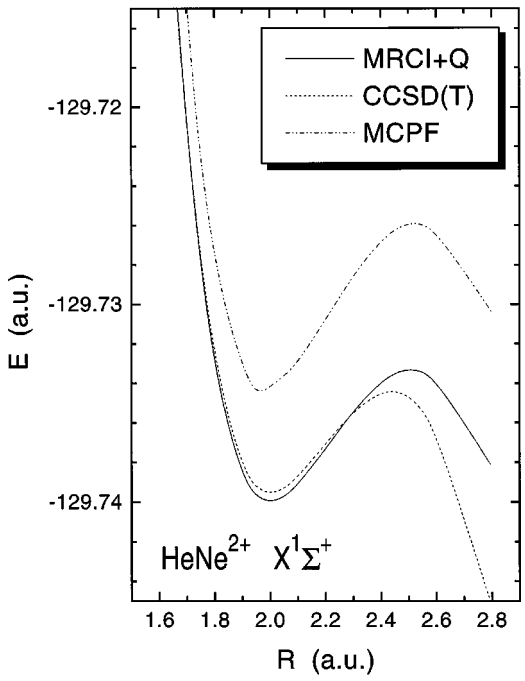

FIG. 2. The potential-energy curves of the $X\,^1\Sigma^+$ electronic ground state of $HeNe^{2+}$ calculated by (i) MRCI+Q (solid line); (b) CCSD(T) (dashed line); and (c) MCPF (dashed-dotted line).

TABLE IV. Total energies (in a.u.) of the $X\,^1\Sigma^+$ ground state of $HeNe^{2+}$ in the metastable region calculated with three different methods.

R (a.u.)	$E_{\mathrm{MRCI}+Q}$	$E_{\mathrm{CCSD}(T)}$	E_{MCPF}
1.60	−129.700 950	−129.701 754	−129.689 111
1.70	−129.722 315	−129.722 295	−129.717 285
1.80	−129.733 859	−129.733 353	−129.728 458
1.90	−129.738 916	−129.738 330	−129.733 205
1.95	−129.739 917	−129.739 302	−129.734 614
2.00	−129.740 206	−129.739 574	−129.734 158
2.05	−129.739 970	−129.739 335	−129.733 632
2.10	−129.739 364	−129.738 745	−129.732 961
2.20	−129.737 557	−129.737 056	−129.730 798
2.30	−129.735 618	−129.735 396	−129.728 529
2.40	−129.734 137	−129.734 406	−129.726 770
2.46	−129.733 638	−129.734 406	−129.726 135
2.50	−129.733 506	−129.734 667	−129.725 926
2.54	−129.733 549	−129.735 176	−129.725 900
2.60	−129.733 958	−129.736 438	−129.726 225
2.80	−129.738 376	−129.745 306	−129.730 418

B. Decay rates

Within the Born-Oppenheimer approximation, the excited bound electronic states of $HeNe^{2+}$ can only decay to the atomic fragments via initial dipole transitions to lower repulsive states, which dissociate spontaneously. Metastable excited states, such as the $F\,^1\Sigma^+$ state, can also decay by tunneling through the potential-energy barrier, while the metastable $X\,^1\Sigma^+$ ground state decays only by tunneling. We have calculated the average decay rate of each vibrational state for each relevant decay mechanism as discussed below in order to find states which agree with the experimental values.

1. Decay by tunneling

Metastable electronic states have a local minimum and thus can decay by tunneling through the potential-energy barrier. The energy of the resonant vibrational states as well as the tunneling decay rate (i.e., the resonance width) have been calculated using the phase-shift method described in detail in our previous work [19]. The mean lifetimes of vibrational states decaying by tunneling decrease rapidly with increasing vibrational quantum number because the barrier they have to tunnel through becomes smaller. It is important to note that typically the mean lifetimes differ by large factors from one vibrational state to the other as can be seen from the exponential dependence in the known WKB tunneling rate formula [20] (in a.u.)

$$\tau_v^{-1} \propto e^{-2\sqrt{2\mu}\int_a^b dR\sqrt{V(R)-E_v}}, \tag{3}$$

where μ is the reduced mass of the molecule, which is of the order of a few thousand a.u. for common diatomic molecules. For example, factors of about three orders of magnitude have been calculated for highly excited vibrational states of $NeAr^{2+}$ in its electronic ground state [19]. Large differences are also expected between the mean lifetimes of

TABLE V. MRCI expansions for different electronic states of $HeNe^{2+}$ at $R=3.0$ a.u.

State	Number of Ref. CSFs	Total number of CSFs in MRCI	Important configurations Occupation [a]	Coefficient [b]	Extra Ref. weight	Mulliken populations (natural MRCI orbitals) [c]
$X\,^1\Sigma^+$	8	201 848	22 022	0.836	0.027	He: 1.03(s); $\Sigma=1.04$
			20 222	−0.522		Ne: 3.99(s), 0.96(p_0),1.99($p_\pm$); $\Sigma=8.96$
$A\,^1\Pi$	3	129 259	22 132	0.987	0.026	He: 1.03(s); $\Sigma=1.04$
						Ne: 3.99(s), 1.95(p_0), 1.00(p_+), 1.99(p_-); $\Sigma=8.96$
$a\,^3\Pi$	3	202 555	22 112	0.985	0.028	He: 1.05(s); $\Sigma=1.07$
						Ne: 3.99(s), 1.92(p_0), 1.00(p_+), 1.99(p_-); $\Sigma=8.96$
$b\,^3\Sigma^+$	3	232 704	21 122	0.987	0.026	He: 1.00(s); $\Sigma=1.01$
						Ne: 3.99(s), 1.00(p_0), 1.99($p_\pm$); $\Sigma=8.99$
$c\,^3\Sigma^-$	1	125 773	22 211	0.990	0.020	He: 1.95(s); $\Sigma=1.96$
						Ne: 4.00(s), 2.00(p_0), 1.00($p_\pm$); $\Sigma=8.04$
$d\,^3\Pi$	3	202 555	12 212	0.971	0.034	He: 1.89(s); $\Sigma=1.90$
			22 112	0.152		Ne: 4.00(s), 1.08(p_0), 1.00(p_+), 1.99(p_-); $\Sigma=8.96$
$B\,^1\Delta$	8	20 148	22 202	0.698	0.026	He: 1.91(s); $\Sigma=1.92$
			22 220	−0.698		Ne: 4.00(s), 0.87(p_0), 1.59($p_\pm$); $\Sigma=8.07$
$C\,^1\Pi$	3	129 259	21 232	0.981	0.030	He: 1.92(s); $\Sigma=1.92$
			22 132	0.087		Ne: 4.00(s), 1.05(p_0), 1.00(p_+), 1.99(p_-); $\Sigma=8.07$
$D\,^1\Sigma^+$	8	201 848	02 222	−0.750	0.031	He: 1.91(s); $\Sigma=1.92$
			13 222	−0.075		Ne: 4.00(s), 0.87(p_0), 1.59($p_\pm$); $\Sigma=8.07$
			20 222	0.060		
			22 202	0.445		
			22 220	0.445		
$E\,^1\Sigma^+$	8	201 848	02 222	0.619	0.025	He: 1.93(s); $\Sigma=1.94$
			20 222	−0.185		Ne: 3.94(s), 1.23(p_0), 1.43($p_\pm$); $\Sigma=8.06$
			22 202	0.526		
			22 220	0.526		
$F\,^1\Sigma^+$	8	201 848	02 222	−0.060	0.045	He: 1.91(s); $\Sigma=1.92$
			13 222	−0.086		Ne: 4.00(s), 0.87(p_0), 1.59($p_\pm$); $\Sigma=8.07$
			12 322	0.051		
			20 222	0.969		
$e\,^3\Sigma^+$	3	232 704	21 122	0.962	0.070	He: 1.08(s); $\Sigma=1.10$
						Ne: 3.05(s), 1.87(p_0), 1.96($p_\pm$); $\Sigma=8.90$
$G\,^1\Sigma^+$	8	201 848	20 222	0.835	0.072	He: 0.84(s); $\Sigma=0.86$
			22 022	-0.476		Ne: 3.24(s), 1.92(p_0), 1.96($p_\pm$); $\Sigma=9.14$

[a]For the three active σ and two active π orbitals. ''2'' denotes double occupation, ''1'' high-spin coupled single occupation, and ''3'' low-spin coupled single occupation.

[b]Only coefficients $|c|>0.05$ are given.

[c]p_0 and p_x denote the σ and π components of the p-type atomic orbitals, the total population is denoted as Σ.

different isotopes of a molecular ion decaying by tunneling, because of the shift of the vibrational energies caused by the different reduced masses μ (see Ref. [4]).

2. Decay by dipole transitions

Excited electronic states can decay by dipole transitions to lower states. These transitions are considered to be vertical, i.e., the nuclear motion is negligible relative to the dipole transition time. Thus, one can use the Born-Oppenheimer approximation. The Franck-Condon principle, on the other hand, is not expected to be valid for $HeNe^{2+}$, because the dipole moments depend strongly on the internuclear distance, R (see Table VI). We have used a simple approximation which takes into account the dependence of the electronic dipole moment on R (for details see Ref. [21]). The average decay rate from any initial state k to any final dissociative state a is

$$\overline{W^s_{ka}}=\int_0^\infty dR\; W^s_{ka}(R)\,|\psi_{v_a}(R)|^2, \tag{4}$$

where the electronic spontaneous decay rate at R, $W_{ka}(R)$, is given by

$$W^s_{ka}=\frac{4}{3}\,\frac{\omega^3_{ka}(R)}{c^3}\,|r_{ka}(R)|^2, \tag{5}$$

where $\omega_{ka}(R)=E_k(R)-E_a(R)$ is the transition frequency, and $r_{ka}(R)$ is the dipole moment. For these calculations the

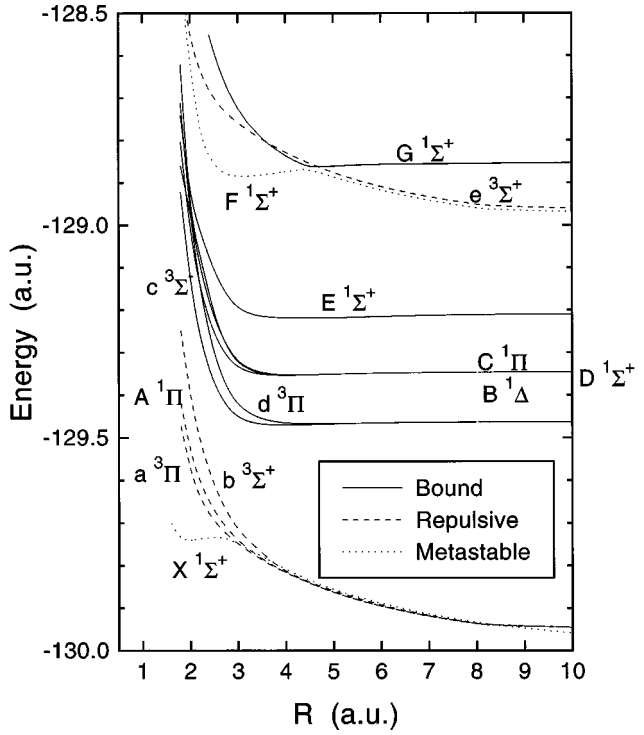

FIG. 3. The potential-energy curves of all the electronic states of $HeNe^{2+}$ calculated by the MRCI+Q method.

wave functions of the vibrational states, $\psi_v(R)$, were evaluated using the Fourier grid method [22].

IV. RESULTS AND DISCUSSION

The potential-energy curves of $HeNe^{2+}$ are shown in Fig. 3 for the dissociation limits listed in Table I. The $X\,^1\Sigma^+$ ground state and the $F\,^1\Sigma^+$ states are metastable, while the other states associated with the $He^+(^2S)+Ne^+(^2P)$ and $He^+(^2S)+Ne^+(^2S)$ dissociation limits are repulsive. All the calculated states correlating with the calculated $He+Ne^{2+}$ asymptotes (II–IV, Table I) are bound by the long-range attractive electrostatic interaction between the Ne^{2+} and the polarized He. Each of these states has a minimum around an internuclear separation of 4–5 a.u. which is deep enough to sustain a few bound vibrational states. The same applies to the $G\,^1\Sigma^+$ state, which correlates with the $He^{2+}+$ Ne dissociation limit. The peculiar shapes of the potential energy curves of the F and G states call for further comment. First, a more technical point: near the local maximum of the F state potential-energy curve, the CAS-SCF orbital optimization procedure failed due to severe root flipping problems. The individual F state energies used for the plot in Fig. 3 were calculated in two separate runs, each approaching the barrier location from shorter and longer internuclear distances, respectively, and using the natural CAS-SCF orbitals from a neighboring point as an initial guess. A slight (about 3 mH) energy difference in the extrapolated barrier locations explains the weak discontinuity in the F state potential-energy curve seen in Fig. 3 around $R=4.5$ a.u. Root flipping and divergence problems for the G state were even more pronounced and could not be solved for internuclear distances $R>3.8$ a.u. Consequently, the long-range potential-energy curve for this state could not be computed using individually optimized orbitals.

To overcome these problems, a second set of calculations of the F and G states was performed, where the natural orbitals, in which the MRCI wave function was expanded, were those from the CAS-SCF calculation of the $X\,^1\Sigma^+$ ground state. In these calculations the $+Q$ correction was not applied, since the ground-state orbitals might be biased against either of the two excited states. The MRCI potential-energy curves, thus obtained, are plotted in Fig. 4. It is clearly recognized that in the adiabatic picture, states F and G, which have the same space and spin symmetry ($^1\Sigma^+$) undergo an avoided crossing at around 4.6 a.u. As a consequence, the F state potential-energy curve exhibits a barrier and is therefore metastable. The minimum and maximum locations are at $R=3.099$ and $R=4.641$ a.u., respectively, and the barrier height amounts to 0.420 eV. This potential well supports five vibrational states for the $^4He\,^{20}Ne^{2+}$ isotope at 424, 1131, 1798, 2419, and 2984 cm^{-1} above its minimum. (These values were calculated neglecting the effect of tunneling on the vibrational levels.) Note that the extremum points lie at almost the same internuclear separations as in the MRCI+Q treatment with individually optimized orbitals, which suggests that the use of the ground-state orbitals for the MRCI expansion of the F state yields physically meaningful results.

Utilizing a diabatic picture, i.e., where no dynamical couplings between the states occur and crossings between potential-energy curves of the same spatial and spin symmetry are allowed, the F state derives from the $He^{2+}+$ Ne asymptote, which is intrinsically attractive due to the charge induced-dipole interaction [2]. Conversely, the G state at shorter internuclear distances derives from the Coulomb-repulsive $Ne^+(^2S,3s^13p^6)+He^+(^2S)$ asymptote. As a consequence of the avoided crossing, the G state potential-energy curve also adopts a bound shape. The total well depth amounts to 9.7 mH, and the minimum is located at around

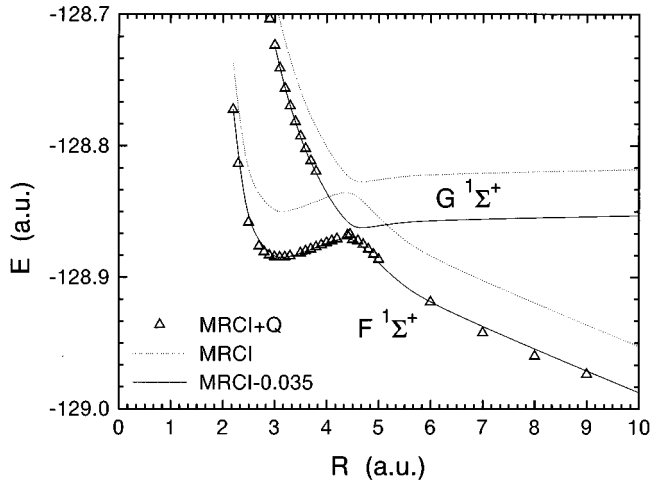

FIG. 4. The potential-energy curves of the F and G electronic states of $HeNe^{2+}$ calculated by MRCI+Q method (symbols) and by MRCI method using the ground state CAS-SCF natural orbitals (lines). (The latter were shifted by -0.035 a.u. in order to match them with the more precise MRCI+Q calculations).

TABLE VI. Transition dipole moments (in a.u.)

From:	$B\,^1\Delta$	$C\,^1\Pi$		$c\,^3\Sigma^-$	$d\,^3\Pi$		
To:	$A\,^1\Pi$	$X\,^1\Sigma^+$	$A\,^1\Pi$	$a\,^3\Pi$	$a\,^3\Pi$	$b\,^3\Sigma^+$	
R(a.u.)							
1.50	0.0163	0.0075	0.6916	0.0360	0.6652	0.0129	
1.60	0.0153	0.0094	0.7329	0.0353	0.7218	0.0103	
1.70	0.0129	0.0108	0.7673	0.0328	0.7725	0.0068	
1.80	0.0098	0.0114	0.7950	0.0294	0.8175	0.0034	
1.90	0.0064	0.0108	0.8156	0.0255	0.8566	0.0001	
2.00	0.0030	0.0105	0.8283	0.0211	0.8892	0.0026	
2.20	0.0034	0.0077	0.8270	0.0123	0.9305	0.0070	
2.50	0.0103	0.0013	0.7601	0.0007	0.9181	0.0110	
2.80	0.0136	0.0050	0.6408	0.0064	0.8241	0.0130	
3.00	0.0142	0.0081	0.5508	0.0090	0.7344	0.0135	
3.50	0.0128	0.0107	0.3460	0.0104	0.4946	0.0124	
4.00	0.0098	0.0091	0.2033	0.0087	0.3012	0.0097	
5.00	0.0045	0.0045	0.0658	0.0042	0.0992	0.0045	
6.00	0.0020	0.0018	0.0204	0.0017	0.0313	0.0018	
7.00	0.0007	0.0007	0.0061	0.0006	0.0097	0.0006	
8.00	0.0002	0.0002	0.0018	0.0002	0.0029	0.0002	
9.00	0.0001	0.0001	0.0005	0.0001	0.0008	0.0001	

From:	$D\,^1\Sigma^+$		$E\,^1\Sigma^+$		$F\,^1\Sigma^+$		$G\,^1\Sigma^+$
To:	$X\,^1\Sigma^+$	$A\,^1\Pi$	$X\,^1\Sigma^+$	$A\,^1\Pi$	$X\,^1\Sigma^+$	$A\,^1\Pi$	$X\,^1\Sigma^+$
R(a.u.)							
1.50	0.8893	0.2663	0.2852	0.0100	0.3044	0.3066	
1.60	0.9475	0.2564	0.3775	0.0317			
1.70	0.9973	0.2420	0.5927	0.0778	0.1829	0.2915	
1.80	1.0435	0.2193	0.8656	0.1269	0.0968	0.2958	
1.90	0.4768	0.0155	1.0881	0.1732	0.0039	0.3017	
2.00	0.1973	0.0348	1.0113	0.1610	0.1092	0.3039	
2.20	0.3081	0.0289	0.9384	0.0808	0.2878	0.2849	
2.50	0.4725	0.0259	0.7794	0.0314	0.4132	0.1987	0.1418
2.80	0.5689	0.0215	0.5827	0.0215	0.4102	0.1022	
2.90							0.3620
3.00	0.5561	0.0181	0.4569	0.0198	0.3759	0.0656	0.3104
3.10							0.2619
3.50	0.3970	0.0113	0.2443	0.0159	0.2615	0.0238	0.1576
3.70							0.1414
4.00	0.2433	0.0075	0.1361	0.0115	0.1667	0.0093	0.1193
4.40					0.1115	0.0045	0.0863
5.00	0.0807	0.0028	0.0437	0.0050			0.0457
5.70							0.0209
6.00	0.0257	0.0010	0.0137	0.0019			
7.00	0.0079	0.0004	0.0042	0.0007			
8.00	0.0024	0.0001	0.0012	0.0002			
9.00	0.0007	0.0000	0.0005	0.0001			

4.7 a.u., which supports 29 vibrational states for the $^4He\,^{20}Ne^{2+}$ isotope, for example. Given all these difficulties, the mean lifetime of the vibrational states bound to the G state are less accurate than those of the other states and they should be considered as estimates only. These estimates are, however, sufficient to compare the calculations with the experimental data (as discussed below).

Now, let us focus on the $X\,^1\Sigma^+$ ground state shown in Fig. 5. This state, according to our calculations, has a much deeper potential well than calculated previously by Montabonel, Cimiraglia, and Persico [2(a)] and others [2(b–d)]. Furthermore, the local minimum of the present potential-energy curve is 0.1743 Hartree lower than the previous one. Note that there is even a qualitative difference between the sets of calculations *while ours sustains a resonant vibrational state, the older ones do not*. The previous potential-energy curve [2(a)] was computed using an MRCI approach based on only four reference configurations, HF-SCF

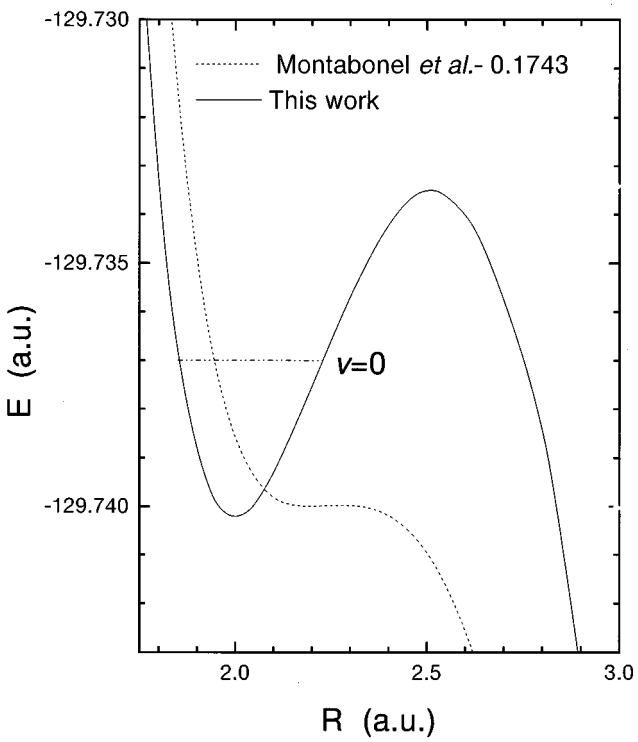

FIG. 5. The calculated $X\,^1\Sigma^+$ ground-state potential-energy curve of $HeNe^{2+}$. Solid line—this work; dashed line from Ref. [2(a)].

orbitals and employing a much less flexible 6–311 G* (i.e., $4s3p1d$ and $3s$ for Ne and He, respectively) one-particle description than in the current investigation. Consequently, the expansion of the MRCI wave function employed in Ref. [2(a)] is significantly less accurate than the one constructed in our present study, leading to the quantitative and qualitative differences between the two sets of calculations. It should be noted that the reason for the occurrence of a barrier in the ground-state potential-energy curve can be attributed in a diabatic picture to an interaction of this state with the high-lying state correlating with the $He^{2+}+$ Ne asymptote as indicated previously by Mercier, Chamband, and Levy [2(d)]. As mentioned above, the metastable ground-state potential-energy curve is deep enough to sustain a single vibrational state which decays by tunneling through the potential-energy barrier. The energy of the $^4He\,^{20}Ne^{2+}$ ground state, $E_{v=0}=-129.737$ a.u., and its mean lifetime, $\tau_{v=0}=11$ ps, have been calculated using the phase-shift method (see Sec. III B). This short mean lifetime makes it impossible to detect the $HeNe^{2+}$ ground state in our measurements. This result is in agreement with the prediction that it is very unlikely to detect the $HeNe^{2+}$ in its ground state made by Frenking *et al.* [3] based on their computed potential-energy curve which agrees well with the results of Montabonel, Cimiraglia, and Persico [2(a)].

TABLE VII. Dipole transition rates and mean lifetimes estimated at R around R_0 of each state.

Initial state	Final state	R (a.u.)	$W^s_{ka}(R)$ (a.u.)	$\tau(R)$ (s)
$B\,^1\Delta$	$A\,^1\Pi$	4.0	4.97×10^{-12}	4.9×10^{-6}
$C\,^1\Pi$	$X\,^1\Sigma^+$	4.0	4.07×10^{-12}	5.9×10^{-6}
	$A\,^1\Pi$	4.0	2.13×10^{-9}	11×10^{-9}
$D\,^1\Sigma^+$	$X\,^1\Sigma^+$	4.0	2.91×10^{-9}	8.3×10^{-9}
	$A\,^1\Pi$	4.0	2.90×10^{-12}	8.3×10^{-6}
$c\,^3\Sigma^-$	$a\,^3\Pi$	4.0	1.64×10^{-12}	15×10^{-6}
$d\,^3\Pi$	$a\,^3\Pi$	5.0	2.03×10^{-9}	12×10^{-9}
	$b\,^3\Sigma^+$	4.0	2.11×10^{-12}	11×10^{-6}
$E\,^1\Sigma^+$	$X\,^1\Sigma^+$	5.0	1.99×10^{-9}	12×10^{-9}
	$A\,^1\Pi$	4.0	1.47×10^{-11}	1.6×10^{-6}
$F\,^1\Sigma^+$ [a]	$X\,^1\Sigma^+$	3.0	4.70×10^{-8}	0.51×10^{-9}
	$A\,^1\Pi$	3.0	1.40×10^{-9}	17×10^{-9}
$G\,^1\Sigma^+$	$X\,^1\Sigma^+$	4.7	2.00×10^{-9}	12.1×10^{-9}

[a]The $F\,^1\Sigma^+$ state can also decay by tunneling (see text).

Tunneling decay rates of isotopes with different reduced masses are expected to vary by large factors as discussed in Sec. III B (see also Ref. [4] for an example calculation). The measured mean lifetimes of the three $HeNe^{2+}$ isotopes are 55 ± 10, 72 ± 14, and 184 ± 32 ns for the (3,20), (3,22), and (4,20) combinations (i.e., $\mu=4775$, 4833, and 6077 a.u.), respectively. These differences are much smaller than those expected for tunneling, suggesting that the long-lived $HeNe^{2+}$ molecular ions decay by dipole electronic transitions to lower dissociating states. This conclusion guided our theoretical search for the appropriate states of each isotope.

The electronic dipole decay rates at a fixed R (around

TABLE VIII. Long-lived states (electronic and vibrational v_f) of $^3He\,^{22}Ne^{2+}$ with decay rates in agreement with the measured ones. The main dissociating state each one decays to by dipole electronic transitions, the main initial vibrational state of the parent $^3He\,^{22}Ne^+$ molecular ion feeding them v_i, and the charge-stripping transition energy E_{trn} (see text).

Decaying $HeNe^{2+}$ state:	$d\,^3\Pi$	$D\,^1\Sigma^+$	$C\,^1\Pi$	$E\,^1\Sigma^+$	$G\,^1\Sigma^+$
v_f	3+4	6,7	6	9+10	5,6
Dipole transitions to state:	$a\,^3\Pi$	$X\,^1\Sigma^+$	$A\,^1\Pi$	$X\,^1\Sigma^+$	$X\,^1\Sigma^+$
Populated from $HeNe^+(v_i)$:	4	2,3	2,3	2	5
E_{trn} (a.u.)	1.51	1.63	1.63	1.77	2.10

TABLE IX. Mean lifetimes of $HeNe^{2+}$ vibrational states (ns).

v	$C\,^1\Pi$	$D\,^1\Sigma^+$	$d\,^3\Pi$	$E\,^1\Sigma^+$
(a) $^3He\,^{20}Ne^{2+}$				
0	12.4	10.8	25.8	28.2
1	14.3	11.5	29.1	23.7
2	17.4	13.3	**36.9**	21.2
3	23.7	18.5	**53.7**	20.3
4	33.1	26.9	98.8	21.2
5	**43.3**	**38.6**	110	23.5
6	**62.5**	**56.8**	181	26.3
7	96.8	87.6	280	29.2
8	153	143	546	32.6
9	272	256	1140	**43.6**
10	533	519	2940	151
11	1260	1310	11 800	205
12	4210	5010		328
13				754
14				2420
(b) $^3He\,^{22}Ne^{2+}$				
v	$C\,^1\Pi$	$D\,^1\Sigma^+$	$d\,^3\Pi$	$E\,^1\Sigma^+$
0	12.4	10.8	25.8	28.2
1	14.3	11.5	29.1	23.7
2	17.4	13.3	36.7	21.1
3	23.6	18.3	**53.1**	20.3
4	32.9	26.6	**97.9**	21.1
5	42.9	38.1	110	23.4
6	**61.5**	**56**	177	26.2
7	95.1	**85.9**	274	29.0
8	149	140	533	32.4
9	263	247	1090	**42.2**
10	508	495	2730	**147**
11	1180	1220	10400	180
12	3772	4430		299
13				705
14				2200
(c) $^4He\,^{20}Ne^{2+}$				
v	$C\,^1\Pi$	$D\,^1\Sigma^+$	$d\,^3\Pi$	$E\,^1\Sigma^+$
0	12.3	10.7	25.6	28.5
1	14.0	11.3	28.3	24.2
2	16.3	12.6	34.2	21.5
3	20.8	15.9	44.6	20.3
4	28.2	22.5	74.8	20.4
5	36.9	30.6	**103**	21.9
6	47.3	43.0	**123**	24.4
7	67.0	61.3	**198**	27.0
8	**98.3**	**90.2**	288	29.5
9	**148**	**139**	516	32.5
10	**245**	**229**	981	39.9
11	429	415	2120	**118**
12	857	866	6040	**117**
13	2100	2290		**265**
14	7540	9830		580
15				1330
16				3980

TABLE X. Mean lifetimes of $HeNe^{2+}$ vibrational states bound to the G electronic state (ns).

v	$^3He\,^{20}Ne^{2+}$	$^3He\,^{22}Ne^{2+}$	$^4He\,^{20}Ne^{2+}$
0	13.2	13.2	13.0
1	20.1	20.0	18.9
2	29.0	28.9	26.3
3	38.7	38.4	34.7
4	**49.8**	49.4	43.7
5	**64.1**	**63.6**	54.8
6	82.2	**81.5**	68.9
7	102	102	85.7
8	129	127	104
9	162	160	128
10	203	200	**156**
11	257	253	**191**
12	327	322	235
13	420	412	291
14	545	533	361
15	715	698	452
16	952	925	570
17	1 286	1 246.	726
18	1 768	1 706.	934
19	2 482	2 385	1 216
20	3 568	3 410	1 606
21	5 273	5 009	2 153
22	8 051	7 593	2 938
23	12 776	11 948	4 089
24	21 205	19 651	5 823
25	31 307	30 611	8 516
26			12 846
27			20 093
28			30 767

R_0), shown in Table VII, have been calculated using Eq. (5) for the $F\,^1\Sigma^+$ metastable state and all the bound electronic states. The estimated mean lifetimes are also shown in the table. For states which have two dipole-transition decay modes the decay rate and mean lifetime of each decay mode was calculated neglecting the other. The mean lifetimes of excited vibrational states are expected to increase with increasing vibrational quantum number v because the nuclear wave functions $\psi_v(R)$ span a wider range of internuclear distances where the dipole moments are typically smaller (see Table VI). The $B\,^1\Delta$ and $c\,^3\Sigma^-$ states have mean lifetimes on the order of μs (see Table VII), and thus do not contribute to the $HeNe^{2+}$ decay measured in our experiments. However, this does not exclude the possibility that they are populated and behave as a ''stable'' fraction in the $HeNe^{2+}$ beam. The metastable $F\,^1\Sigma^+$ state decays much faster to the $X\,^1\Sigma^+$ ground state than to the excited $A\,^1\Pi$ state. Neglecting the slower decay mode a mean lifetime of 0.51 ns is estimated at the local minimum of this state. Thus one expects the mean lifetime of the ground vibrational state to be about 0.5 ns. The excited vibrational states are expected to have only slightly longer mean lifetimes because the potential well has a much shorter range relative to the bound electronic states, and as a result smaller changes in the dipole moments. Furthermore, the highly excited vibrational

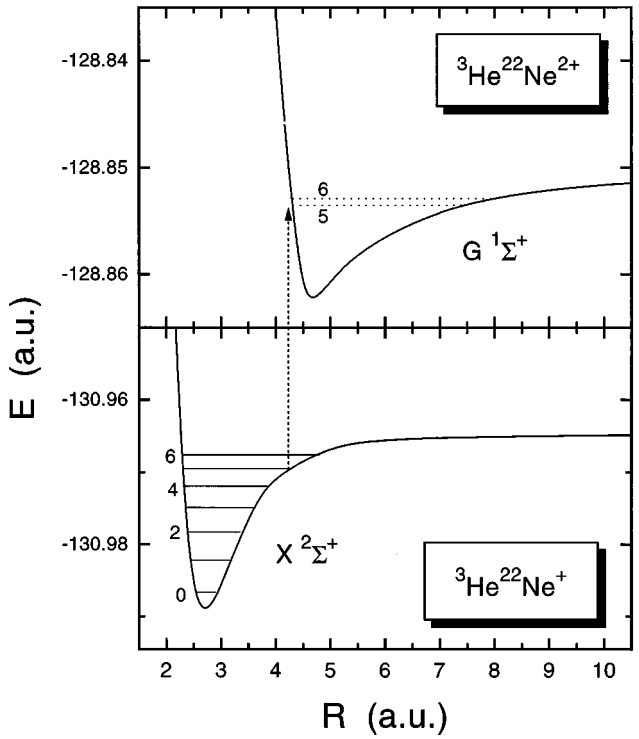

FIG. 6. The possible vertical transition from the electronic ground state of the parent $^3He\,^{22}Ne^+$ populating the $v_f=5,6$ vibrational states of the $G\,^1\Sigma^+$ state of the dication, which have mean lifetimes in agreement with experiment. Note, that this transitions originate mainly from the $v_i=5$ vibrational state.

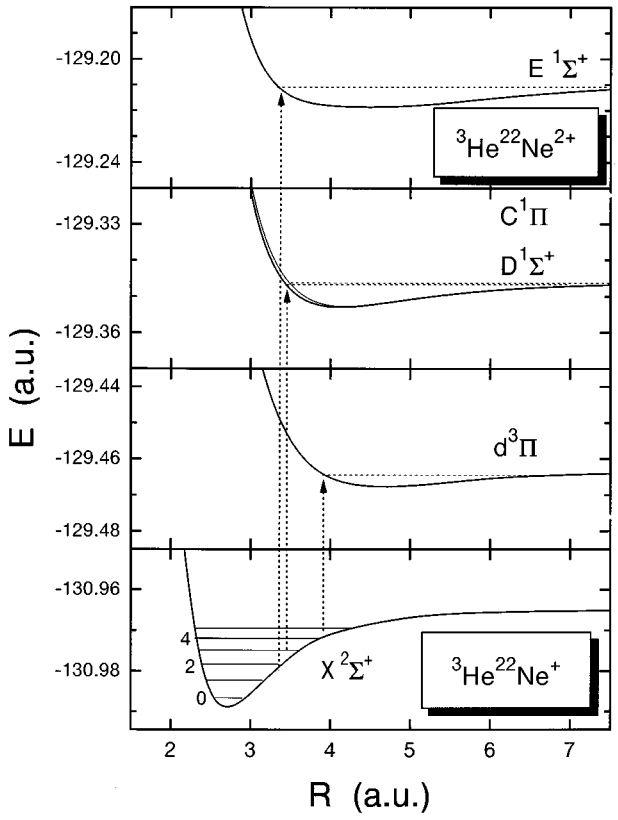

FIG. 7. The possible vertical transitions from the $^3He\,^{22}Ne^+$ ground state to the $d\,^3\Pi$, $C\,^1\Pi$, $D\,^1\Sigma^+$, $E\,^1\Sigma^+$ states of the dication which have mean lifetimes in agreement with experiment.

states may decay even faster by tunneling through the potential-energy barrier, thus reducing the mean lifetimes of these states. Thus, the $F\,^1\Sigma^+$ state decays much faster, and the $B\,^1\Delta$ and $c\,^3\Sigma^-$ states much slower, than the measured rates.

The estimated mean lifetimes around R_0 of the $d\,^3\Pi$, $C\,^1\Pi$, $D\,^1\Sigma^+$, $E\,^1\Sigma^+$, and $G\,^1\Sigma^+$ states suggest that the mean lifetimes of some of the vibrational states bound in these potential wells might be in agreement with the experimental values. The mean lifetimes of these states in the $^3He\,^{22}Ne^{2+}$ isotope have been calculated as explained in Sec. III B taking into account only the fast decay mode shown in Table VIII. The calculated mean lifetimes of all vibrational states are shown in Tables IX and X for all measured isotopes. Some of the vibrational states (printed in bold face) are in good agreement with the measured decay rates shown in Fig. 1 for all measured isotopes and for all these electronic states. Note, that for the $d\,^3\Pi$ and $E\,^1\Sigma^+$ states of the $^3He\,^{22}Ne^{2+}$ isotope, only a mixture of the 3+4 and 9+10 vibrational states, respectively, is in agreement with the experimental decay rate. Thus, it is indicated that dipole electronic transitions to lower dissociating states are the decay mechanism of the measured long-lived $HeNe^{2+}$ molecular ions. However, the question *which of the bound excited electronic states is populated in the charge-stripping collisions,* is still open. Vibrational states with shorter mean lifetimes will dissociate in flight before the analyzer and thus will not be detected. On the other hand, vibrational states with longer mean lifetimes will reach the detector before their decay and will, in practice, be detected as ''stable'' $HeNe^{2+}$. However, by looking only at the He fragments from the dissociation of the long-lived $HeNe^{2+}$ we have chosen to ignore the ''stable'' molecular ions, i.e., we focused on a narrow window of mean lifetimes.

In the charge-stripping collisions a vertical transition from the $HeNe^+$ parent molecular ions populates the vibrational states of the long-lived $HeNe^{2+}$ molecular ions, whose decay we observed experimentally. Consider, for example, Figs. 6 and 7 for the case of the $^3He\,^{22}Ne^{2+}$ isotope: In the first figure it is shown that collisions which populate the $v_f=5$, 6 vibrational states bound to the $G\,^1\Sigma^+$ electronic state originate preferentially from the $v_i=5$ state of the parent molecular ion. This is due to the required overlap between the initial and final vibrational wave functions. In the second figure we show the respective vertical transitions to populate the vibrational states of interest of the remaining four electronic states which may have been measured. In Table VIII we summarize the information we have about the states with calculated mean lifetimes in agreement with experiment. The energy needed for the transition E_{exc} is also given in the table. Using the information listed in Table VIII one can argue that the $G\,^1\Sigma^+$ state should be the least likely of the five to be populated in the charge-stripping collisions because a higher excitation energy is needed. Furthermore, this state is populated from the highest initial vibrational state which is typically a smaller fraction of the incoming $HeNe^+$ beam, because singly charged molecular ions produced in rf ion sources, like the one used in our accelerator, typically have a Boltzmann distribution of vibrational states with an effective temperature of a few thousand degrees, thus

the fraction of $HeNe^+$ molecular ions in a given vibrational state v_i falls off with increasing v_i.

The situation for the other four states is more complicated. For example, the $d\,^3\Pi$ state is populated from a higher vibrational state of the parent $HeNe^+$ than the $C\,^1\Pi$, $D\,^1\Sigma^+$, and $E\,^1\Sigma^+$ states, which originate from roughly the same initial vibrational states. On the other hand, the excitation energy needed for the charge-stripping transition is lowest for the $d\,^3\Pi$ state, and thus, the lowest transition energy favors the $d\,^3\Pi$ state over the others while the initial vibrational state feeding it is least populated. Therefore, qualitative arguments based on the charge-stripping mechanism forming the long-lived $HeNe^{2+}$ cannot help to exclude any of these states, even the $G\,^1\Sigma^+$ state which is expected to be the least likely according to the argument given above cannot be excluded because the transition energy and initial population differences are not that large. Thus the number of possible electronic states associated with the measured long-lived $HeNe^{2+}$ molecular ions cannot be reduced from five. In order to determine the relative population of each of these long-lived states in the charge-stripping collisions additional measurements are needed, such as spectroscopy of the emitted photons or measurements of the kinetic energy released upon dissociation. Given the very low rate for $HeNe^{2+}$ production (typically, a few per second) the latter approach is more promising. Another possible approach is to conduct a quantitative theoretical study of the transition probabilities to the different electronic states of $HeNe^{2+}$ in fast $HeNe^+ + Ar$ collisions, and by that determine the relative importance of these long-lived states.

Finally, note that out of the five possible electronic states, three have the same $^1\Sigma^+$ symmetry as the electronic ground state. Thus, the argument used commonly that long-lived excited electronic states which decay via initial dipole electronic transitions should have a different symmetry than the dissociating states below them is not always valid.

V. SUMMARY

The mean lifetimes of two additional isotopes of the long-lived $HeNe^{2+}$ molecular ion were measured. The massive $^4He\,^{20}Ne^{2+}$ isotope has the longest mean lifetime 184 ± 32 ns, while the mean lifetimes of the lighter isotopes are closer to each other, 55 ± 10 ns for $^3He\,^{20}Ne^{2+}$, and 72 ± 14 ns for $^3He\,^{22}Ne^{2+}$. The similarity between the latter is due to their reduced masses being much closer to each other than to the reduced mass of $^4He\,^{20}Ne^{2+}$. Our calculations indicate that the $d\,^3\Pi$, $C\,^1\Pi$, $D\,^1\Sigma^+$, $E\,^1\Sigma^+$, and $G\,^1\Sigma^+$ electronic states of $HeNe^{2+}$ have vibrational states which decay at rates consistent with the measured decay rate for all isotopes measured. These states decay by dipole transitions to lower dissociating states, a decay mechanism for which only small isotopic effects are expected. Additional measurements are needed to determine the relative population of these long-lived states in $HeNe^+ + Ar$ charge-stripping collisions. Finally, the new calculations of the $X\,^1\Sigma^+$ ground electronic state indicate that it is metastable in contrast to being unbound as predicted in previous calculations. However, the only vibrational resonance in the ground-state potential-energy curve has a mean lifetime of ~ 11 ps, too short to be detected in our measurements.

ACKNOWLEDGMENTS

This work was supported in part by the Division of Chemical Sciences, Office of Basic Energy Sciences, Office of Energy Research, U.S. Department of Energy, and in part by the Foundation for promotion of research at the Technion, and in part by Fonds der Chemischen Industrie.

[1] I. Ben-Itzhak, I. Gertner, O. Heber, and B. Rosner, Chem. Phys. Lett. **212**, 467 (1993).

[2] (a) M.C.B. Montabonel, R. Cimiraglia, and M. Persico, J. Phys. B **17**, 1931 (1984); (b) **21**, 185 (1985); (c) R. Cimiraglia, J.-P. Malrieu, M. Persico, and F. Spiegelmann, *ibid.* **18**, 3073 (1985); (d) E. Mercier, G. Chambaud, and B. Levy, *ibid.* **18**, 3591 (1985).

[3] G. Frenking, W. Koch, D. Cremer, J. Gauss, and J.F. Liebman, J. Phys. Chem. **93**, 3397 (1989).

[4] I. Ben-Itzhak, J.P. Bouhnik, Z. Chen, I. Gertner, C. Heinemann, W. Koch, C.D. Lin, and B. Rosner, Phys. Rev. A **52**, R3401 (1995), and **54**, 981 (1996).

[5] I. Gertner, I. Ben-Itzhak, and B. Rosner, Nucl. Instrum. Methods Phys. Res. B **94**, 47 (1994).

[6] (a) E.P. Wigner and E.E. Witmer, Z. Phys. **51**, 859 (1928). (b) G. Herzberg, *Molecular Spectra and Molecular Structure Vol. I. Spectra of Diatomic Molecules* (Krieger Reprint Edition, Malabar, FL 1991).

[7] B.O. Roos, Adv. Chem. Phys. **69**, 399 (1987); and in *Lecture Notes in Quantum Chemistry* , edited by B.O. Roos, Lecture Notes in Chemistry Vol. 58 (Springer, Berlin 1992).

[8] For a detailed description of the method see P.E.M. Siegbahn, in *Lecture Notes in Quantum Chemistry*, (Ref. [7]).

[9] (a) E.R. Davidson, in *The World of Quantum Chemistry*, edited by R. Daudel and B. Pullmann (Reidel, Dordrecht, 1974); (b) S.R. Langhoff and E.R. Davidson, Int. J. Quantum Chem. **8**, 61 (1974); (c) E.R. Davidson and D.W. Silver, Chem. Phys. Lett. **52**, 403 (1977).

[10] (a) J. Almlöf and P.R. Taylor, J. Chem. Phys. **86**, 4070 (1987); (b) P.-O. Widmark, B.J. Perrson, and B.O. Roos, Theor. Chim. Acta **79**, 419 (1991).

[11] (a) P.-Å. Malmqvist, Int. J. Quantum Chem. **30**, 479 (1986); (b) P.-Å. Malmqvist and B.O. Roos, Chem. Phys. Lett. **155**, 189 (1989).

[12] MOLCAS-2, MOLCAS-3: K. Anderson, M.R.A. Blomberg, M.P. Fülscher, V. Kellö, R. Lindh, P.-Å. Malmqvist, J. Noga, J. Olsen, B.O. Roos, A.J. Sadlej, P.E.M. Siegbahn, M. Urban, and P.-O. Widmark, University of Lund, Sweden (1991 and 1994).

[13] C.E. Moore, *Atomic Energy Levels*, Natl. Bur. Stand. Circ. No. NSRDS-NBS 35 (U.S. GPO, Washington, DC, 1971).

[14] (a) P.R. Taylor, T.J. Lee, J.E. Rice, and J. Almlöf, Chem. Phys. Lett. **163**, 359 (l989); (b) D.P. Chong and S.R. Langhoff, J. Chem. Phys. **93**, 570 (1990); (c) J.E. Rice, P.R. Taylor, T.J.

Lee, and J. Almlöf, *ibid.* **94**, 4972 (1991).
[15] See the discussion in: (a) J. Wasilewski, V. Staemmler, and S. Koch, Phys. Rev. A **38**, 1289 (1988); (b) B. Gemein, R. de Vivie, and S.D. Peyerimhoff, J. Chem. Phys. **93**, 1165 (1990).
[16] Recent reviews: (a) R.J. Bartlett, J. Phys. Chem. **93**, 1697 (1989); (b) R.J. Bartlett and J.F. Stanton, in *Reviews in Computational Chemistry*, edited by K.B. Lipkowitz and D.B. Boyd (VCH, New York 1994), Vol. 5; (c) P.R. Taylor, in *Lecture Notes in Quantum Chemistry*, II, edited by B. O. Roos, *Lecture Notes in Chemistry* Vol. 64. (Springer, Berlin, 1995).
[17] D.P. Chong and S.R. Langhoff, J. Chem. Phys. **84**, 5606 (1986).
[18] See, AIP Document No. E-PAPS.E-PLRAAN-56-1268 to recall the tabulated potential-energy curves E-PAPS document files may be retrieved free of charge from our FTP server (http://www.aip.org/epaps/html). For further information: e-mail: paps@aip.org or fax: 516-576-2223.
[19] Z. Chen, I. Ben-Itzhak, C.D. Lin, W. Koch, G. Frenking, I. Gertner, and B. Rosner, Phys. Rev. A **49**, 3472 (1994).
[20] E. Merzbacher, *Quantum Mechanics* (Wiley, New York, 1961).
[21] I. Ben-Itzhak, Z. Chen, B.D. Esry, I. Gertner, O. Heber, C.D. Lin, and B. Rosner, Phys. Rev. A **49**, 1774 (1994).
[22] C.C. Marston and G.G. Balint-Kurti, J. Chem. Phys. **91**, 3571 (1989).
[23] Experimental values taken from *CRC Handbook of Chemistry and Physics*, 68th ed., edited by R.C. Weast (Chemical Rubber Co., Boca Raton, FL, 1987).